Atmos. Chem. Phys. Discuss., 4, 969–989, 2004
www.atmos-chem-phys.org/acpd/4/969/
SRef-ID: 1680-7375/acpd/2004-4-969

Atmospheric Chemistry and Physics Discussions

Simultaneous lidar observations of temperatures and waves in the polar middle atmosphere on both sides of the Scandinavian mountains: a case study on 19/20 January 2003

U. Blum[1], **K. H. Fricke**[1], **G. Baumgarten**[2], **and A. Schöch**[2]

[1]Physikalisches Institut der Universität Bonn, D-53115 Bonn, Germany
[2]Leibniz-Institut für Atmosphärenphysik e.V., D-18225 Kühlungsborn, Germany

Received: 9 January 2004 – Accepted: 23 January 2004 – Published: 11 February 2004

Correspondence to: U. Blum (blum@physik.uni-bonn.de)

Abstract

Atmospheric gravity waves have been the subject of intense research for several decades because of their extensive effects on the atmospheric circulation and the temperature structure. The U. Bonn lidar at the Esrange and the ALOMAR RMR lidar at the Andøya Rocket Range are located in northern Scandinavia 250 km apart on either side of the Scandinavian mountain ridge. During January and February 2003 both lidar systems conducted measurements and retrieved atmospheric temperatures. On 19/20 January 2003 simultaneous measurements for more than 7 h were possible. Although during most of the campaign time the atmosphere was not transparent for the propagation of orographically induced gravity waves, they could propagate and were observed at both lidar stations during these simultaneous measurements. The wave patterns at ALOMAR show a random distribution with time whereas at the Esrange a persistency in the wave patterns is observable. This persistency can also be found in the distribution of the most powerful vertical wavelengths. The mode values are both at about 5 km vertical wavelength, however the distributions are quite different, narrow at the Esrange containing values from λ_z=2–6 km and broad at ALOMAR, covering λ_z=1–12 km vertical wavelength. At both stations the waves deposit energy in the atmosphere with increasing altitude, which leads to a decrease of the observed gravity wave potential energy density with altitude. These measurements show unambigiously orographically induced gravity waves on both sides of the mountains as well as a clear difference of the characteristics of these waves, which might be caused by different excitation and propagation conditions on either side of the Scandinavian mountain ridge.

1. Introduction

It is well established that atmospheric waves of different scales and types play a key role in driving the global circulation and thus influencing the temperature structure of the atmosphere (e.g. Fritts and Alexander, 2003). The formation of polar stratospheric

ACPD

4, 969–989, 2004

clouds (PSCs) in the northern hemisphere is often driven by gravity wave induced cooling (Carslaw et al., 1998) when the synoptic scale temperatures are a few Kelvin above the formation temperature of PSCs. These waves can be excited orographically by surface obstacles and the Scandinavian mountain ridge is a major source (Størmer, 1929; Volkert and Intes, 1992). The Scorer parameter must decrease with altitude for the propagation of mountain waves from the ground up to the stratosphere and even higher (Scorer, 1949). Thus the propagation of gravity waves can be inhibited by the background wind field. Strong disturbances of the horizontal wind field occur during major stratospheric warmings (Scherhag, 1952; Matsuno, 1971) which are regularly observed in the polar winter stratosphere (Labitzke and Naujokat, 2000).

The U. Bonn lidar at the Esrange and the ALOMAR RMR lidar at the Andøya Rocket Range are both well equipped to retrieve atmospheric temperature profiles from about 30 km to roughly 80 km altitude with a time resolution of 1 h. These profiles regularly show temperature disturbances which can be identified as atmospheric internal gravity waves.

In January and February 2003 a field campaign took place to investigate the impact of the Scandinavian mountain ridge on atmospheric gravity waves. The U. Bonn lidar and the ALOMAR RMR lidar performed measurements whenever permitted by the weather conditions, to maximise the chance for simultaneous measurements. Due to different meteorological situations at both stations – affected by the Scandinavian mountain ridge – the tropospheric cloud coverage differs extremely, thus opportunities for simultaneous measurements are rare. Nevertheless a total of nine simultaneous measurements were obtained during the campaign. Although one minor and one major stratospheric warming occurred at the beginning of January as well as one minor warming in the middle of February leading to critical level filtering in the troposphere and lower stratosphere, on several days wave signatures were observed in the middle stratosphere at both lidar stations. On 19/20 January 2003 a simultaneous data set of more than 7 h duration was obtained. These data and the accompanying wave analysis are presented here.

ACPD
4, 969–989, 2004

2. Data set

The U. Bonn lidar is located at the Esrange (68° N, 21° E) near the Swedish city of Kiruna. The ALOMAR RMR lidar is located next to the Andøya Rocket Range (69° N, 16° E) 250 km to the north-west of the Esrange. Between both stations the Scandinavian mountain ridge is a major source for the excitation of mountain waves. During polar winter eastward winds regularly dominate the mean horizontal flow in the troposphere and stratosphere. Thus we expect to observe different wave patterns upstream (ALOMAR) and downstream (Esrange) of the mountains.

The U. Bonn lidar and the ALOMAR RMR lidar both use a pulsed Nd:YAG solid state laser as light source. The backscattered light from the atmosphere is collected by telescope systems, detected by photomultipliers, and recorded by counting electronics (Müller et al., 1997; von Zahn et al., 2000). The elapsed time between emission of a light pulse and detection of the echo determines the scattering altitude. In the aerosol free part of the atmosphere (i.e. typically above 30 km altitude) the backscattered light is proportional to the molecular number density. Assuming hydrostatic equilibrium, the integration of the range corrected lidar net signal yields the temperature profile. At the upper end of the profile a seed temperature has to be estimated, which we take from the MSISE90 (Hedin, 1991) or CIRA86 (Fleming et al., 1990) model, respectively. The altitude resolution of both lidar systems is 150 m, however, smoothing of the raw data before temperature calculation reduces this altitude resolution to about one kilometer. The time resolution is determined by the integration time of the lidar data. Longer integration times result in temperature profiles reaching higher altitudes having higher precision but losing time resolution. This is a well known trade-off in all lidar systems.

Here lidar data were integrated for 1 h with a shift of 15 min in the starting point resulting in a number of individual, though not fully independent profiles for each measurement night. The integration for the complete night results in a mean temperature profile, which reaches higher up and shows less wave structure than the individual profiles.

ACPD
4, 969–989, 2004

During the campaign in January/February 2003, the U. Bonn lidar conducted 29 measurement runs, lasting from less than 1 h up to more than 61 h with continuous data. During this period the ALOMAR RMR lidar performed 16 measurement runs with durations from about 1 h up to 26 h. In total we performed nine simultaneous measurement runs lasting from half an hour up to more than 7 h. During the night of 19/20 January the U. Bonn lidar started with measurements on 19 January at 14:21 UT, ending on 20 January at 10:18 UT, whereas the ALOMAR RMR lidar measurements lasted from 19 January, 19:28 UT to 20 January, 02:40 UT. Thus we have 7.2 h of simultaneous measurements on this night which will be discussed here.

3. Method

The first step in data processing is to subtract the night mean temperature profile from the individual profiles to obtain the residuals, which are then identified as the wave induced variations. For the wave analysis we use the power spectrum and the gravity wave potential energy density of the observed waves as well as the maximum vertical wavelength, which can penetrate through the atmosphere.

We Fourier transform the profiles of residuals and calculate the power spectrum, which result in the vertical wavelength spectra. We use Parseval's theorem to normalise the power spectra, and finally we calculate the amplitude of a given wave by multiplying the square-root of the power spectrum coefficient $f(k_z)$ by the vertical wavenumber k_z. Thus we can derive the dominant vertical wavelengths of the observed spectra.

Time series of the residual profiles can be used to calculate the gravity wave potential energy density per volume ($GWPED_{\mathrm{vol}}$), given by

$$GWPED_{\mathrm{vol}}(z) = \frac{1}{2}\frac{g^2(z)}{N^2(z)}\overline{\left(\frac{\Delta T(z)}{\overline{T(z)}}\right)^2}\, n(z)\,\overline{m}. \qquad (1)$$

ACPD
4, 969–989, 2004

This quantity consists essentially of the time mean of the squared relative temperature variation $\overline{\left(\Delta T(z)/\overline{T(z)}\right)^2}$, where $\Delta T(z)$ is the temperature perturbation and $\overline{T(z)}$ is the night mean temperature profile. This quantity is further multiplied by a stability factor $g^2(z)/N^2(z)$, where $g(z)$ is the acceleration due to gravity and $N(z)$ the Brunt-Väisälä frequency. The symbol $n(z)$ stands for the atmospheric number density which is taken from the lidar measurement. The range-corrected net signal is directly proportional to the atmospheric number density. The calibration factor is found through comparison with ECMWF analyses. Finally $\overline{m}$ is the mean molecular mass of the atmosphere. The $GWPED_{\mathrm{vol}}$ is a measure of the potential energy available in a gravity wave and can be used to estimate energy dissipation with altitude. In case of energy conservation in an ascending wave, the value of the $GWPED_{\mathrm{vol}}$ is constant with altitude.

To estimate the transparency of the atmosphere for vertically propagating gravity waves we use ECMWF T106 analysis data provided by the Norwegian Institute for Air Research (NILU) on 28 pressure levels from ground up to the lower mesosphere. Using the simplified dispersion relation

$$k_z = \frac{2\pi}{\lambda_{\max}} = \frac{N}{|\overline{u_h} - c_{ph}|} \tag{2}$$

(e.g. Fritts, 1984), where $\overline{u_h}$ is the mean horizontal wind in the direction of wave propagation and c_{ph} the horizontal phase velocity of the wave, allows us to calculate the maximum vertical wavelength $\lambda_{\max}$ which can propagate through the atmosphere. Critical levels imply that $\lambda_{\max}$ approaches zero. For vertically ascending mountain waves the horizontal phase velocity is $c_{ph} = 0$ m/s. Thus the maximum vertical wavelength $\lambda_{\max}$ can be written as

$$\lambda_{\max}(z) = \overline{|u(z)_h|} P_B(z) \tag{3}$$

where $P_B = 2\pi/N$ is the Brunt-Väisälä period. Due to the fact that the propagation direction of the waves is not determinable by the single location measurements of the

ACPD
4, 969–989, 2004

lidar stations, we will consider two selected, orthogonal states in the following: 1. The waves propagating zonally and 2. the waves propagating meridionally.

4. Meteorological background

The temperature profiles retrieved by the two lidar systems during the whole campaign period provide an overview of the mean atmospheric temperature structure above northern Scandinavia in early 2003 (Fig. 1). Due to the alternating good measurement conditions at both lidar stations we have a nearly complete temperature coverage for the time period January/February 2003. These nightly mean temperature profiles show a similar structure on a coarse scale on both sides of the mountains but the details reveal differences. The ALOMAR RMR lidar was operating from 2 January onward and could observe a first stratospheric warming during 2 and 3 January. A second warming on 15–17 January was observed by both lidar instruments. Although the temperatures observed with the ALOMAR RMR lidar show higher values during the first warming than during the second, the hemispheric view asserts that the first warming was a minor warming, whereas the second event was a major stratospheric warming, including a wind reversal (Naujokat and Grunow, 2003). In the beginning of the lidar campaign the ALOMAR RMR lidar measured stratopause temperatures of up to 309 K at an altitude of about 43 km. High stratopause temperatures of 280 K where observed at about 45 km altitude by both lidars during 15–17 January. Following this warming unusually cold temperatures in the altitude range of 30–50 km were observed during an eight day period. In the beginning of February the atmosphere was almost isothermal from about 40–65 km altitude during a six day period (5–11 February) as is typical for the final recovery stage of major warmings observed early in January (Labitzke, 1971).

This inhomogeneous temperature structure combined with the wind pattern leads to critical level filtering during nearly the entire campaign period. Figure 2 shows the calculated critical levels, using ECMWF T106 analyses for January and February 2003 at Kiruna. Plotted is the maximum vertical wavelength λ_{max} which can penetrate through

ACPD
4, 969–989, 2004

the atmosphere. Red regions mean large values for λ_{max}, i.e. the atmosphere is transparent, whereas dark blue and black regions indicate critical levels which inhibit propagation of (orographically induced) gravity waves. Due to the reduced vertical resolution of about 1 km both lidars cannot detect gravity waves with vertical wavelengths shorter than 2 km. The atmosphere was transparent for mountain waves during the stratospheric warmings on the first weeks of January above 35 km altitude, but waves were not able to penetrate through the lower and middle stratosphere up to this altitude. This situation changed directly after the major warming and led to a more transparent middle and lower stratosphere. However, critical levels occurred around the stratopause altitude. From the beginning of February onwards, the middle and lower stratosphere were again dominated by critical levels, thus mountain waves were not able to ascend from the ground or even from the troposphere into the stratosphere and mesosphere.

Considering the meteorological background situation, the long simultaneous measurement on 19/20 January 2003 by both lidar systems took place exactly during the period in which critical level filtering decreased in the lower atmosphere and the chance increased for mountain waves to propagate up to the stratopause.

5. Observations on 19/20 January 2003

Figure 3 shows the individual temperature profiles for the night 19/20 January 2003, measured by the ALOMAR RMR lidar (left plot) and the U. Bonn lidar (right plot), respectively, during the simultaneous measurements. Temperature profiles from 19 January are plotted in red, those from 20 January in blue. Although throughout most of the campaign time critical level filtering inhibited wave propagation, strong wave activity is found in all individual profiles on both stations covering the whole observed altitude range from 30–65km. Variations in the temperature of several 10 K appear. Obviously during the measurements of this case study critical level filtering did not occur. While the observed wave structure varies all the time above ALOMAR, the Esrange data show two distinct profile types. Around midnight the wave system above the Esrange

ACPD
4, 969–989, 2004

changes which can be most clearly seen around 35 km, 43 km, and 48 km altitude, where the temperature variation shows a phase jump leading to a change in temperature of about 15 K.

For all profiles we calculated spectra of the vertical wavelength λ_z. Figure 4 shows the distribution of the dominant vertical wavelengths of the individual spectra. The histograms show two different distribution patterns. The mean value for the distribution at ALOMAR is 6.3 km and hence much larger than the mean at the Esrange of 4.4 km. The difference between median and mean is much smaller for the Esrange data than for the ALOMAR data which is consistent with the different shapes of the distributions. Whereas the distribution at ALOMAR ranges from λ_z=1–12 km, that at the Esrange covers mainly values from λ_z=2–6 km. In fact the distribution at ALOMAR seems to comprise two different distributions, one dominant with a mean value at about 5 km and a second, less pronounced around 10 km vertical wavelength. Thus the wave spectrum at the Esrange is more narrow than at ALOMAR which indicates less variability in the waves above the Esrange. The prominent persistency of the wave pattern in the Esrange data seen in Fig. 4 in comparison to the ALOMAR data is thus also represented in the spectra.

From the residual profiles we derived the gravity wave potential energy density per volume, using Eq. (1). Figure 5 shows the potential energy density measured at both stations. The coarse structure is quite similar at both sides of the mountains up to an altitude of 50 km. The $GWPED_{\mathrm{vol}}$ decreases from about 0.5 J/m^3 near 30 km by a factor of 50 to values of 0.01 J/m^3 near 50 km altitude. In the altitude range above 50 km the mean potential energy density stays constant on both sides of the mountains, with about 0.01 J/m^3 at the Esrange and 0.005 J/m^3 at ALOMAR. The measurements show unambigously that the observed waves deposit energy with increasing altitude in the 30–50 km altitude region.

Figure 6 shows the maximum vertical wavelengths λ_{max} (see Eq. 3) for waves which can propagate through the atmosphere derived from ECMWF T106 wind data, for purely zonal (left plot) and meridional (right plot) propagation directions, respectively.

ACPD
4, 969–989, 2004

ECMWF T106 analyses are available every 6 h of which we use data for 19 January, 18:00 UT, 20 January, 00:00 UT and 06:00 UT. According to the ECMWF analyses the atmospheric conditions were quite similar at both stations. With the present instrumental setup and the data analysis the lidars cannot observe gravity waves with vertical wavelengths shorter than 2 km. Thus a quasi critical level is reached if λ_{max} falls below 2 km. In the lower troposphere the wind direction and speed created critical level filtering in the 2–3 km altitude range for both zonally and meridionally propagating waves. Between ALOMAR and the Esrange the highest mountain – in fact the highest mountain of the whole Scandinavian mountain ridge – extends to well above 2000 m. Consequently we consider only those critical levels as relevant which exist above the mountains, thus at altitudes above 3 km. Higher up in the troposphere at about 10 km altitude a critical level for meridionally propagating waves evolved above ALOMAR on 20 January, 06:00 UT; however throughout the stratosphere meridionally propagating waves were able to propagate all times. Maximum vertical wavelengths of $\lambda_{max} \approx 10$ km indicate this. Different from the meridionally moving waves, zonally propagating gravity waves reached a critical level already at about 35 km altitude. Higher up the maximum propagable vertical wavelength stayed constant with values of about 2–4 km.

6. Discussion

On 19/20 January 2003 the ALOMAR RMR lidar and the U. Bonn lidar both observed wave signatures in the temperature profiles up to 65 km altitude. The $GWPED_{vol}$ was very similar on both sides of the mountains, showing a strong decrease in potential energy density from 30 to 50 km altitude. Thus the propagation conditions in the upper stratosphere and lower mesosphere were similar on both sides of the mountains, leading to this decrease in wave energy above 30 km altitude. The observed decrease of the $GWPED_{vol}$ does not agree with the maximum vertical wavelength λ_{max}, derived from ECMWF data for zonally propagating gravity waves, however it is compatible

ACPD
4, 969–989, 2004

with meridionally propagating gravity waves. Whereas the zonally propagating gravity waves die out above 35 km, meridionally propagating gravity waves can reach altitudes of about 50 km before λ_{max} decreases. Thus the propagation direction of the observed gravity waves must be close to meridional. This is consistent with the ECMWF analyses which indicate winds from the north at 3 km altitude leading to mostly meridionally propagating gravity waves (Pavelin and Whiteway, 2002). Analogous to the $GWPED_{vol}$ the maximum vertical wavelength λ_{max} must decrease. Filtering of waves with longer wavelengths reduces the total number of propagating waves and thus the total amount of potential energy transported by the gravity waves.

On the other hand the observed individual profiles as well as the distribution of the dominant vertical wavelengths reveal large differences between both stations. The more random distribution of the wave signatures in the temperature profiles at ALOMAR indicate that there was no major source exciting "monochromatic" gravity waves. In fact, each local orographical obstacle around Andøya may lead to gravity waves, thus ALOMAR observes probably a superposition of waves coming from different sources. A change in the excitation at individual sources due to changes in the local boundary layer wind field can thus lead to changing wave pattern as observed at ALOMAR. In contrast to ALOMAR at the Esrange the wave pattern stays essentially constant in time, which indicates a constant excitation at a dominant wave source such as the Scandinavian mountain ridge. Obviously the change in the lower tropospheric winds and hence the changing excitation of mountain waves at the Esrange is not as prominent as at ALOMAR. These observations clearly demonstrate that gravity waves can be observed up- and downwind of the mountain ridge, showing different characteristics which are caused by different excitation and propagation conditions on either side of the mountains. The observed change in the temperature profiles above Esrange around midnight is an obvious indication of a modification of the propagation conditions for gravity waves around midnight.

Figure 7 shows the ECMWF mean horizontal wind speeds $\overline{u}$ for ALOMAR (left panel) and Esrange (right panel) at three different times covering the observation period of

both lidars. The wind profiles are rather constant during the measurement time of the lidars. Only the last wind profiles of 20 January, 06:00 UT show initial stages of a tropospheric jet at about 8 km altitude. This jet is more pronounced at Esrange with a horizontal wind speed of about 45 m/s than at ALOMAR with 30 m/s. The tropospheric jet might cause a change in the propagation conditions for atmospheric gravity waves above the Esrange or act as additional wave source resulting in the observed change of the individual temperature profiles around midnight.

7. Summary

On 19/20 January 2003 we obtained more than 7 h of simultaneous lidar measurements using the U. Bonn lidar at the Esrange and the ALOMAR RMR lidar at the Andøya Rocket Range, 250 km apart on either side of the Scandinavian mountains. Gravity wave signatures were detected in the temperature profiles of both stations. Whereas the gravity wave potential energy density per volume shows very similar characteristics on both sides of the mountains the observed temperature profiles as well as the distributions of the dominant vertical wavelengths reveal large differences. The ECMWF wind data indicate that there were no critical levels for meridionally propagating mountain waves up to the stratopause. The random-like distribution of wave pattern with time at ALOMAR indicates variable excitation conditions whereas the persistent wave structure at the Esrange suggests a constant excitation of mountain waves. Further the appearance of a tropospheric jet might be closely connected to a change on the observed wave structure above the Esrange. The observations clearly demonstrate the presence of gravity waves of comparable amplitude up- and downwind of the mountains while a homogeneous and continuous gravity wave field is present only on the downwind side of the Scandinavian mountain ridge.

Acknowledgements. We thank the staffs of the Esrange and the Andøya Rocket Range for their always quick and uncomplicated support during the measurement campaigns. The measurements at ALOMAR were supported by the “Access to the ALOMAR research infrastructure”

project of the European Union. The measurements at the Esrange were funded by the Envisat Validation project granted by the DLR Erdbeobachtung FKZ 50 EE 0009. Finally we like to thank the NILU for providing the ECMWF T106 analysis data.

References

Carslaw, K. S., Wirth, M., Tsias, A., Luo, B. P., Dörnbrack, A., Leutbecher, M., Volkert, H., Renger, W., Bacmeister, J. T., Reimer, E., and Peter, T.: Increased stratospheric ozone depletion due to mountain-induced atmospheric waves, Nature, 391, 675–678, 1998. 971

Fleming, E. L., Chandra, S., Barnett, J. J., and Corney, M.: Zonal mean temperature, pressure, zonal wind, and geopotential height as function of latitude, Adv. Space Res., 10, 12, 11–59, 1990. 972

Fritts, D. C.: Gravity wave saturation in the middle atmosphere: A review of theory and observations, Rev. Geophys., 22, 3, 275–308, 1984. 974

Fritts, D. C. and Alexander, M. J.: Gravity wave dynamics and effects in the middle atmosphere, Rev. Geophys., 41, 1, 1003, doi:10.1029/2001RG000106, 2003. 970

Hedin, A. E.: Neutral atmosphere empirical model from the surface to the lower exosphere MSISE90, J. Geophys. Res., 96, 1159–1172, 1991. 972

Labitzke, K.: Temperature changes in the mesosphere and stratosphere connected with circulation changes in winter, J. Atmos. Sci., 29, 756–766, 1971. 975

Labitzke, K. and Naujokat, B.: The lower Arctic stratosphere in winter since 1952, SPARC Newsletter, 15, 11–14, 2000. 971

Matsuno, T.: A dynamical model of the stratospheric sudden warming, J. Atmos. Sci., 28, 1479–1494, 1971. 971

Müller, K.-P., Baumgarten, G., Siebert, J., and Fricke, K. H.: The new lidar facility at Esrange, Kiruna, Proceedings of the 13th ESA symposium on European Rocket and Ballon Programmes and Related Research, Öland 1997, Sweden, ESA-SP-397, 129–134, 1997. 972

Naujokat, B. and Grunow, K.: The stratospheric Arctic winter 2002/03: Balloon flight planning by trajectory calculations, Proceedings of the 16th ESA symposium on European Rocket and Ballon Programmes and Related Research, St. Gallen 2003, Switzerland, ESA-SP-530, 421–425, 2003. 975

Pavelin, E. and Whiteway, J. A.: Gravity wave interactions around the jet stream, Geophys. Res. Lett., 29, doi:10.1029/2002GL015783, 2002. 979
Scherhag, R.: Die explosionsartige Stratosphärenerwärmung des Spätwinters 1951/1952, Ber. Deut. Wetterdienst, 6, 51–62, 1952. 971
Scorer, R. S.: Theory of mountain waves of large amplitude, Quart. J. R. Met. Soc., 75, 41–56, 1949. 971
Størmer, C.: Remarkable clouds at high altitudes, Nature, 123, 260–261, 1929. 971
Volkert, H. and Intes, D.: Orographically forced stratospheric waves over northern Scandinavia, Geophys. Res. Lett., 19, 1205–1208, 1992. 971
von Zahn, U., von Cossart, G., Fiedler, J., Fricke, K. H., Nelke, G., Baumgarten, G., Rees, D., Hauchecorne, A., and Adolfsen, K.: The ALOMAR Rayleigh/Mie/Raman lidar: Objectives, configuration, and performance, Ann. Geophys., 18, 815–833, 2000. 972

ACPD
4, 969–989, 2004

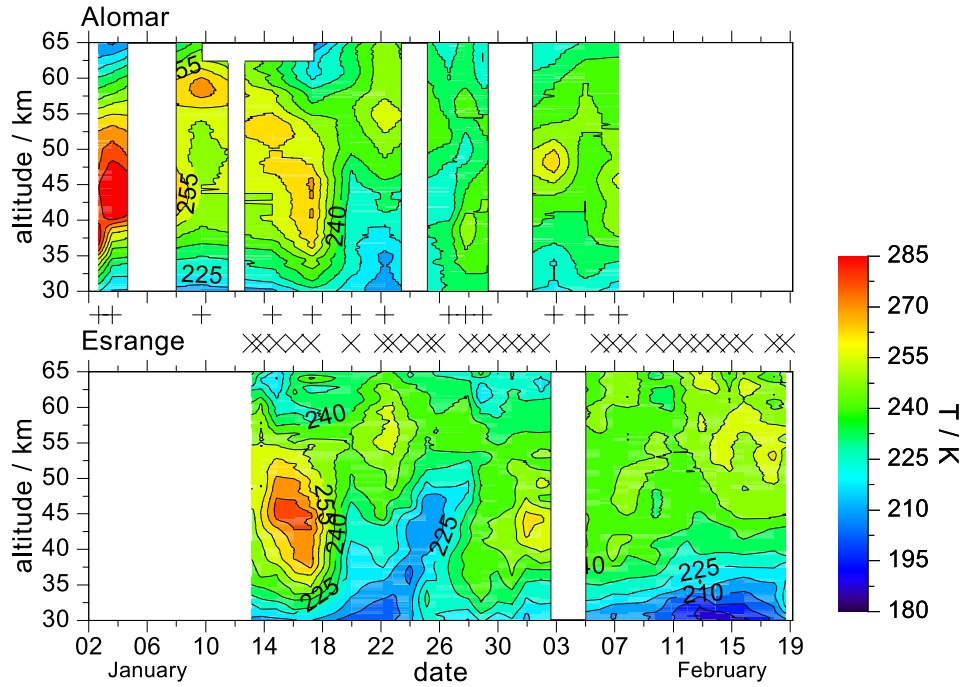

Fig. 1. Temperature development observed by the ALOMAR RMR lidar in Norway (upper row) and the U. Bonn lidar at the Esrange in Sweden (lower row) for January and February 2003. The abscissa shows the date of January/February 2003, the ordinate the altitude in kilometers, and the color code the temperature in Kelvin. Measurement times are marked by "+"-signs for ALOMAR data and "×"-signs for Esrange data.

ACPD
4, 969–989, 2004

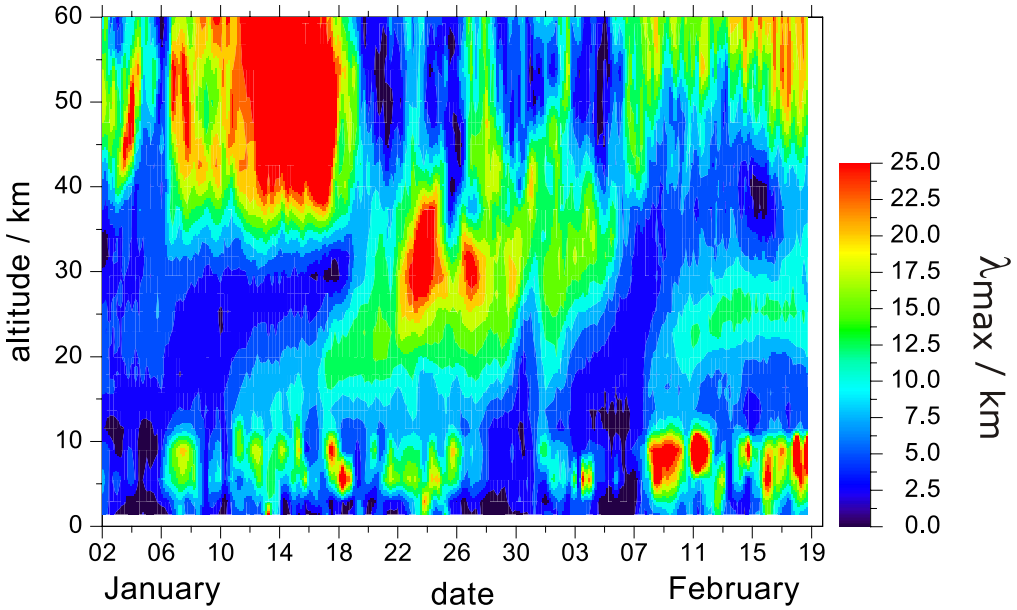

Fig. 2. Critical level calculation for Esrange with ECMWF T106 data. The abscissa shows the date on January/February 2003, the ordinate the altitude and the color code the maximum vertical wavelength λ_{max}, which can penetrate through the respective atmospheric level. Dark blue areas are critical levels which inhibit vertical propagation of internal gravity waves.

ACPD
4, 969–989, 2004

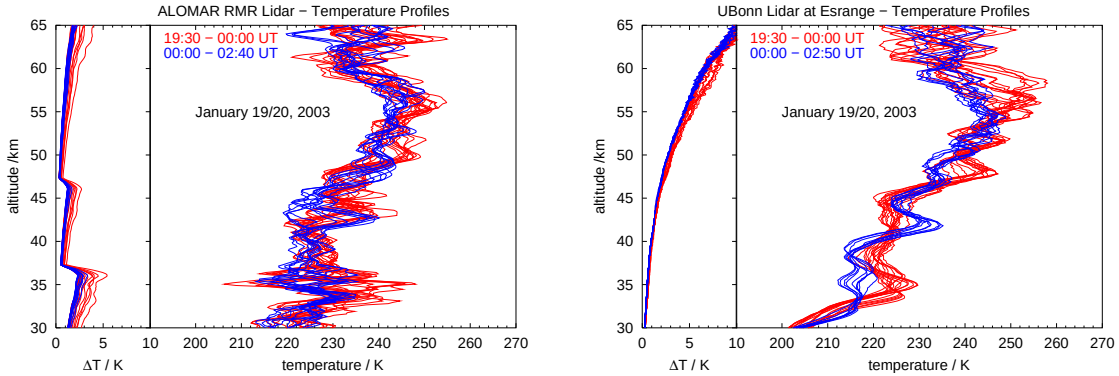

Fig. 3. Temperature profiles for 19/20 January 2003 measured by the ALOMAR RMR lidar (left plot) and the U. Bonn lidar (right plot). Shown are temperature profiles of 1 h integration time. The starting points of the integrations are shifted by 15 min. The left part of each plot presents the temperature errors for each individual profile.

ACPD
4, 969–989, 2004

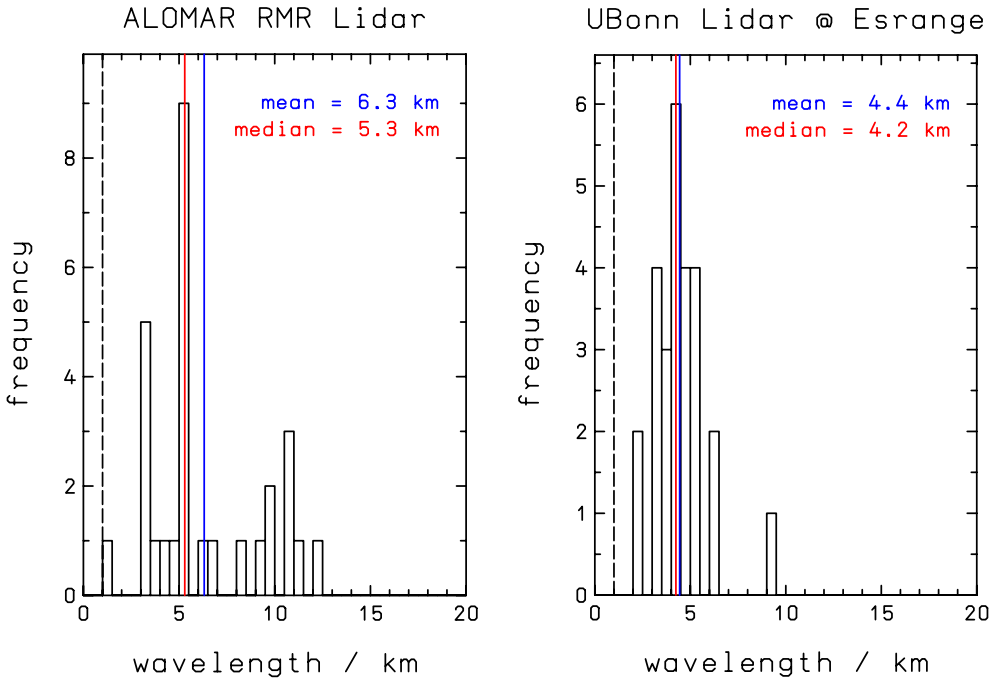

Fig. 4. Distribution of dominant vertical wavelengths at ALOMAR (left panel) and the Esrange (right panel) during the measurement night 19/20 January 2003. The abscissa gives the dominant vertical wavelength in km and the ordinate the absolute occurence rate of the respective wavelength. The mean and median values of the distribution are also given.

ACPD
4, 969–989, 2004

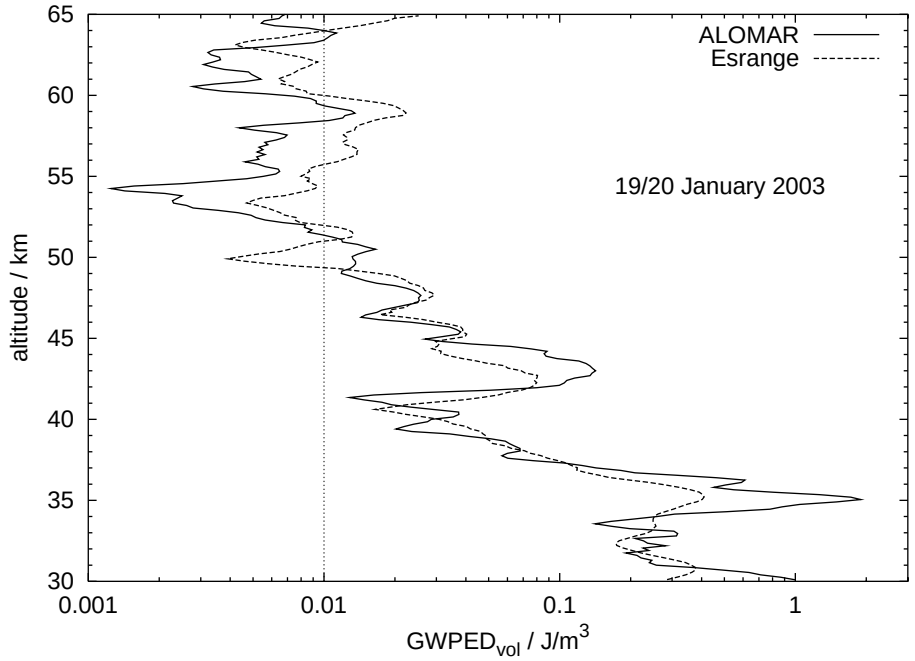

Fig. 5. Gravity wave potential energy density measured at ALOMAR and at the Esrange. ALOMAR data are shown by the solid line, the dashed line represents the Esrange profile.

ACPD

4, 969–989, 2004

Simultaneous lidar observations of temperatures and waves

U. Blum et al.

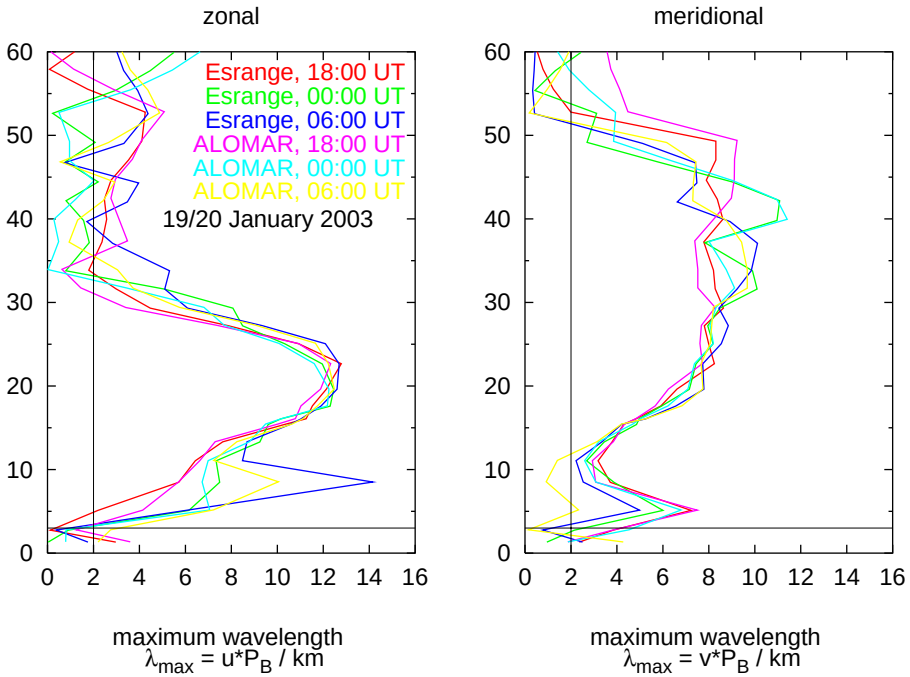

Fig. 6. Atmospheric transparency for mountain waves derived from ECMWF T106 analyses for 19/20 January 2003. Shown are the maximum vertical wavelengths λ_{max} which can penetrate through the atmosphere for purely zonally (left plot) and purely meridionally propagating gravity waves (right plot). Horizontal lines at 3 km mark the minimum altitude for critical levels that are of relevance and the vertical lines at 2 km mark the minimum wavelength observable by the lidar instruments.

ACPD
4, 969–989, 2004

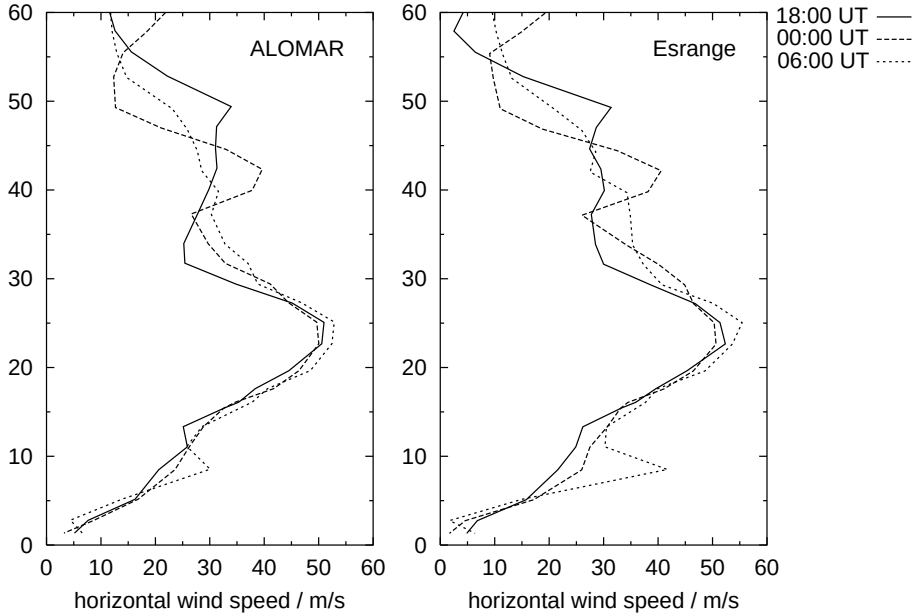

Fig. 7. ECMWF T106 data for 19/20 January 2003. Shown is the mean horizontal wind speed $\overline{u}$. The left panel contains the data for ALOMAR, the right one those for Esrange. Data are for 19 January, 18:00 UT (solid line), 20 January, 00:00 UT (dashed line) and for 20 January, 06:00 UT (dotted line).

ACPD
4, 969–989, 2004